Draft version March 8, 2017
Preprint typeset using LaTeX style AASTeX6 v. 1.0

arXiv:1703.02234v1 [astro-ph.GA] 7 Mar 2017

THE DEPENDENCE OF CLUSTER GALAXY PROPERTIES ON THE CENTRAL ENTROPY OF THEIR HOST CLUSTER

Jae-Woo Kim[1], Jongwan Ko[1,2], Ho Seong Hwang[3], Alastair C. Edge[4], Joon Hyeop Lee[1,2], Jong Chul Lee[1], and Hyunjin Jeong[1]

[1]Korea Astronomy and Space Science Institute, 776 Daedeokdae-ro, Yuseong-gu, Daejeon 34055, Republic of Korea
[2]University of Science and Technology, Daejeon 34113, Republic of Korea
[3]School of Physics, Korea Institute for Advanced Study, 85 Hoegiro, Dongdaemun-gu, Seoul 02455, Republic of Korea
[4]Centre for Extragalactic Astronomy, Durham University, South Road, Durham DH1 3LE, UK

ABSTRACT

We present a study of the connection between brightest cluster galaxies (BCGs) and their host galaxy clusters. Using galaxy clusters at $0.1 < z < 0.3$ from the Hectospec Cluster Survey (HeCS) with X-ray information from the Archive of *Chandra* Cluster Entropy Profile Tables (ACCEPT), we confirm that BCGs in low central entropy clusters are well aligned with the X-ray center. Additionally, the magnitude difference between BCG and the 2nd brightest one also correlates with the central entropy of the intracluster medium. From the red-sequence (RS) galaxies, we cannot find significant dependence of RS color scatter and stellar population on the central entropy of the intracluster medium of their host cluster. However, BCGs in low entropy clusters are systematically less massive than those in high entropy clusters, although this is dependent on the method used to derive the stellar mass of BCGs. In contrast, the stellar velocity dispersion of BCGs shows no dependence on BCG activity and cluster central entropy. This implies that the potential of the BCG is established earlier and the activity leading to optical emission lines is dictated by the properties of the intracluster medium in the cluster core.

Keywords: galaxies: clusters: general — galaxies: elliptical and lenticular, cD — galaxies: formation — galaxies: evolution — galaxies: kinematics and dynamics

1. INTRODUCTION

Under the Λ cold dark matter (ΛCDM) paradigm, the dark matter halo evolves hierarchically from small density fluctuations to large cluster-like structures. A galaxy cluster represents the most massive dark matter halo or a density peak in the universe. In addition, since it is also believed that galaxies form and evolve at the center of dark matter halos (White & Rees 1978), the formation and evolution of galaxies are significantly affected by the property of host dark matter halos (e.g., Baugh 2006).

In this context, the correlations between properties of brightest cluster galaxies (BCGs), usually located at the center of galaxy clusters, and their host galaxy clusters allow us to understand the environmental effect of the host clusters on the formation and evolution of the central galaxies. However, many results have reported that the position of BCG and the center of X-ray emission is not always coincident. Also, the amount of offset is well correlated with the property of galaxy clusters. BCGs in galaxy clusters with low central entropy values or cooling flow are well aligned with the X-ray centers, but those with high central entropy or distorted X-ray morphology show the larger offset between them (Sanderson et al. 2009; Hoffer et al. 2012; Groenewald & Loubser 2014; Hashimoto et al. 2014).

Another interesting aspect of BCGs is their star formation and nuclear activity. BCGs are regarded as the most massive galaxies in the universe and hence host the most massive Black Holes and largest stellar populations. However, the fraction of BCGs show emission lines in their spectra or blue optical colors, which are different from the widely adopted properties of red, passive early-type galaxies at low redshift. The BCGs with emission lines (active BCGs, hereafter) usually show a small separation from the X-ray center (Crawford et al. 1999; Sanderson et al. 2009), and reside in galaxy clusters with low central entropy or short cooling time, that are considered as cool-core clusters (Cavagnolo et al. 2008; Rafferty et al. 2008; Wang et al. 2010; Pipino et al. 2011; Hoffer et al.

kjw0704@kasi.re.kr

2012; Fogarty et al. 2015). They also show color excesses at UV and mid-IR regimes (Donahue et al. 2010; Hoffer et al. 2012; Green et al. 2016). Moreover, it is known that active BCGs show dust (Edge et al. 1999; Rawle et al. 2012), warm molecular hydrogen (Edge et al. 2002; Egami et al. 2006), CO emission (Edge 2001; Salomé & Combes 2003), and atomic cooling lines (Edge et al. 2010; Mittal et al. 2012). All this evidence supports the star formation activity or the existence of active galactic nuclei (AGN) in active BCGs, and these are related to the intracluster medium of host clusters.

It is expected that the comparison between BCGs and other cluster galaxies provides an opportunity to understand the evolutionary stage of galaxy clusters or the evolution history of BCGs, since BCGs are dominant galaxies in galaxy clusters in terms of brightness and mass (Ostriker & Tremaine 1975; Loh & Strauss 2006). For example, Green et al. (2016) find that active BCGs tend to show larger magnitude difference from the 2nd brightest one than passive BCGs without emission lines, which is consistent with Lauer et al. (2014). However, studies are still not enough to draw a firm conclusion regarding the correlations between BCGs and other cluster galaxies due to the lack of deep spectroscopy confirming the enough number of member galaxies.

As already mentioned, since galaxies evolve in their host dark matter halos, the stellar mass (or luminosity) of central galaxies is tightly connected to the halo mass (Zheng et al. 2007; Behroozi et al. 2010; Moster et al. 2010; Wake et al. 2011; Kim et al. 2015). In addition, the relation between them is related to the efficiency of conversion from baryons to stars, and important to constrain galaxy formation and evolution models. The galaxy clusters are also good laboratories to directly measure the stellar mass-halo mass ratio (Lin & Mohr 2004; Gonzalez et al. 2007; Hansen et al. 2009; Kravtsov et al. 2014; Hwang et al. 2016).

In this work, we use galaxy clusters at $0.1 < z < 0.3$ from the Hectospec Cluster Survey (HeCS, Rines et al. 2013) with X-ray information from the Archive of *Chandra* Cluster Entropy Profile Tables (ACCEPT, Cavagnolo et al. 2009). This is one of the best datasets to study the interrelation between member galaxies and their host clusters, since we can use a large number of spectroscopically confirmed members with broad-band photometry and uniformly analyzed X-ray information. Using this, we investigate the dependence of the property of cluster galaxies on that of host clusters, and address the relation between masses of central galaxies and galaxy clusters.

In § 2, we introduce datasets about cluster sample, photometry/spectroscopy and properties of galaxies and clusters. Then main results and discussion are presented in § 3. Finally, we conclude the results in § 4. In this paper, the photometry is in AB magnitude system and we assume H_0 =70 km s^{-1} Mpc^{-1}, Ω_m =0.3 and Ω_Λ =0.7.

2. DATA

2.1. *Cluster Sample*

The HeCS clusters were selected from the ROSAT All-Sky Survey (Voges et al. 1999) with the Sloan Digital Sky Survey Data Release 6 (SDSS DR6, Adelman-McCarthy et al. 2008) footprint. Then, the spectroscopic follow-up observation was performed with the Hectospec instrument on MMT. Finally, 58 galaxy clusters at $0.1 < z < 0.3$ were surveyed. From the spectra of mainly red-sequence galaxies, Rines et al. (2013) defined bona fide cluster members through the caustic technique (Diaferio & Geller 1997; Diaferio 1999) and provided cluster information such as redshift, r_{200}, M_{200}, velocity dispersion ($\sigma_v^{\rm cl}$) and so on. r_{200} is the radius satisfying that the density is 200 times the critical density and M_{200} is a mass within r_{200}. The caustic method is advantageous to estimate the cluster mass, because the algorithm is based on both galaxy kinematics and positions without assuming dynamical equilibrium, and accurately recovers the mass profile up to several Mpc (Diaferio 1999; Serra et al. 2011).

To investigate the dependence of member galaxy properties on the central entropy of galaxy clusters, we cross-match the HeCS clusters with those in ACCEPT, which provides well measured X-ray properties. We mainly adopt the central entropy of the intracluster medium (K_0) from ACCEPT (Cavagnolo et al. 2009). Based on the X-ray center of each cluster, the radial profiles of temperature and electron density were estimated. Then, the radial entropy profile was calculated using the estimated temperature and electron density profiles. Finally, the value of K_0 was estimated by fitting the model including a power-law for large radii and a constant value for small radii to the calculated entropy profile. Of 58 HeCS clusters, 29 clusters overlap with the ACCEPT clusters, and we focus on these clusters in this work. Table 1 lists 29 clusters and information from HeCS and ACCEPT.

2.2. *Spectroscopic/Photometric Data*

As already mentioned, Rines et al. (2013) applied the caustic technique to define the members of galaxy clusters. Here, we adopt spectroscopic redshift and membership of galaxies in galaxy clusters from their result. We complement this data with a spectroscopic sample of galaxies from SDSS DR12 (Alam et al. 2015) and with redshifts in the literature (see Hwang et al. 2010,

for details). The galaxy clusters used in this work have more than 100 members confirmed spectroscopically, except Zw2701 that has 93 members. Note that the distribution of members spans out to a few Mpc in order to fully sample the caustic profile.

In addition to the spectroscopic information, photometric information is also important to estimate stellar mass. Since all galaxy clusters are covered by the SDSS footprint, we use *ugriz* model magnitudes to estimate the color of galaxies and r-band cmodel magnitude for the total magnitude from the SDSS DR12. Using the dust map from Schlegel et al. (1998), we also correct the Galactic extinction for each galaxy. Finally, the absolute magnitude at z =0.1 is calculated with including the K-correction (Blanton & Roweis 2007) and the evolution correction (Tegmark et al. 2004) in this work (see also Hwang et al. 2012).

2.3. *Galaxy Properties*

The main purpose of this work is to investigate the association between cluster galaxies and host galaxy clusters. Therefore, added to the cluster properties described, it is necessary to use the property of member galaxies such as stellar mass ($M_*^{\rm BCG}$) and stellar velocity dispersion ($\sigma_v^{\rm BCG}$) for BCGs. To gauge the stellar mass of BCGs, we use three different measurements for the comparison between different methodologies.

First, to estimate stellar masses of BCGs (see § 3.1.1 for BCG identification), we run the Fitting and Assessment of Synthetic Templates (FAST, Kriek et al. 2009) code with the Conroy et al. (2009) stellar population synthesis model. We also assume a Chabrier (2003) initial mass function, the Calzetti et al. (2000) dust attenuation curve, and a delayed star formation history (star formation rate $\propto \tau e^{-\tau/t}$). $\log\tau$/yr ranges from 8 to 10 with the step size of 0.1 dex, and the age ranges from 100 Myr to the universe age of each galaxy with $\Delta\log {\rm t} = 0.02$. Finally, the internal dust extinction (A_V) is set between 0 and 5 with a 0.05 increment, and the metallicity is allowed to have 0.04, 0.16, 0.51, 1.00 and 1.58 $Z_\odot$.

Second, we also use the stellar mass from Maraston et al. (2013) to compare the result with different models. They performed spectral energy distribution (SED) fitting with two different templates, passive and star formation ones. Although they use Salpeter (1955) and Kroupa (2001) initial mass functions, we adopt stellar masses derived with a Kroupa (2001) initial mass function. After cross-matching BCGs with their catalog, we compare χ^2 values from both templates, and then the stellar masses with smaller χ^2 are selected. In total, 23 BCGs are included in their catalog with only 6 BCGs (A1068, A1413, A1689, RXJ1504, A2034 and A2259) missing.

Finally, stellar masses and velocity dispersion of BCGs from the MPA/JHU value-added catalog[1] are used as well. The stellar masses were measured by the similar scheme to Kauffmann et al. (2003), but SDSS photometry with correcting for the contribution of nebular emission was used instead of spectral indices. In this catalog, 21 BCGs are contained. Absent BCGs are in A773, A1413, A1423, A1689, A1763, A2034, A2219 and A2259. The stellar velocity dispersion in the MPA/JHU catalog is from Princeton/MIT SDSS spectroscopy[2]. Among our BCGs, 19 BCGs are in the catalog with velocity dispersion values measured. The values are listed in Table 2. In order to make the values measured by the consistent physical scale, we apply the aperture correction with the relation in Montero-Dorta et al. (2016). Also, to minimize the influence of emission lines and blue continuum, the effective radius for z-band is adopted from the New York University Value-added Galaxy Catalog (Blanton et al. 2005a,b) for the correction.

3. RESULTS AND DISCUSSION

3.1. *Brightest Members*

3.1.1. *BCG Identification*

In order to select BCGs, we initially use the spectroscopic samples only. Among galaxies with spectroscopic redshifts, we select the brightest galaxy at r-band within a 1 Mpc radius from the X-ray center of each cluster and within the relative rest-frame radial velocity of $\pm$ 2000 km s^{-1} from the cluster redshift. Then, they are inspected whether there are brighter galaxies from SDSS. Finally, we define BCGs if there is no brighter galaxy within the velocity range. In the case of A1758, there are two candidates with similar brightnesses and redshifts, but one of them is located in the different X-ray peak from that used in ACCEPT. Thus, we select the closer one to the X-ray center of ACCEPT. We also note that most BCGs defined are consistent with those in Hoffer et al. (2012), except A1758, A1914 and A2069. Their BCGs were identified using near-IR images and redshift information from archives. They selected the galaxy in the another X-ray peak for A1758, but we use BCG which is closer to the X-ray center in ACCEPT. On the other hand, for the others, our BCGs are brighter than theirs in optical and near-IR bands, and we use the latest redshift information from SDSS DR12 and HeCS.

Using the positions of BCGs selected and the X-ray centers from ACCEPT, we calculate the projected offset between those for each cluster. The coordinate of

[1] http://wwwmpa.mpa-garching.mpg.de/SDSS/DR7/ http://home.strw.leidenuniv.nl/~jarle/SDSS/

[2] http://spectro.princeton.edu/

BCGs and the calculated offsets are listed in Table 2. Figure 1 displays the X-ray/BCG offset (top) and the offset normalized by the cluster radius (bottom) against the central entropy (K_0) of clusters used in this work. In order to investigate the dependence on the X-ray morphology, we also use the measurement of morphological parameters (symmetry, peakiness and alignment) in Mantz et al. (2015). They provided criteria of each parameter to classify galaxy clusters, and the relaxed clusters were defined when all parameters satisfy the criteria. Among our sample, 24 clusters have measurements. The color code in Figure 1 represents the number of parameters satisfying their criteria, i.e., blue points are relaxed clusters in Mantz et al. (2015). The satisfied parameters for each cluster are noted in Table 1. The dotted line indicates K_0 =30 keV cm^2 which is known to distinguish galaxy clusters hosting active and passive BCGs (Cavagnolo et al. 2008). In fact, from SDSS and literature spectroscopy all 8 BCGs in galaxy clusters with K_0 <30 keV cm^2 show emission lines, and that in Zw2701 with K_0 =39.66 keV cm^2 also shows the emission lines. On the other hand, all 20 BCGs in K_0 >50 keV cm^2 clusters are known to be passive galaxies without emission lines (Cavagnolo et al. 2008). Open triangles in the bottom panel denote BCGs whose spectra are available from SDSS. Overall, it is confirmed that active BCGs with emission lines (open circles in the top panel) are relatively well aligned with the X-ray centers. In addition, all relaxed clusters in Mantz et al. (2015) have active BCGs. On the other hand, BCGs in galaxy clusters with K_0 >30 keV cm^2 show a trend that BCGs in high K_0 clusters are more misaligned from the X-ray centers. These are in good agreement with previous results (Katayama et al. 2003; Sanderson et al. 2009; Hoffer et al. 2012).

3.1.2. *Dominance of BCGs*

The luminosity difference between BCG and the 2nd brightest member is regarded as an indicator of the possibility of recent halo mergers or the formation epoch (Smith et al. 2010). Here, we compare the magnitude gap with the central entropy of clusters.

In order to identify 2nd brightest galaxies, we apply the same scheme to the first step for the BCG identification, except using the radius of r_{200} and checking galaxies with brightnesses between BCGs and selected 2nd brightest candidates. We also inspect if there are brighter galaxies within the velocity range of the caustic profile. From these, we securely identify the 2nd brightest galaxies in 22 galaxy clusters, which are spectroscopic members without other brighter galaxies (group A in Table 2). In the case of rest of the clusters, there are brighter galaxies than the 2nd brightest ones, but their spectroscopic information is absent. For 2nd brightest galaxies without spectroscopic redshifts, we use photometric redshift information from SDSS (Beck et al. 2016). If the redshift difference between the cluster redshift and the photometric redshift is larger than 0.129 corresponding to three times the uncertainty of photometric redshifts[3], we select the original candidate from the first step as the 2nd brightest one (group B). On the other hand, if the redshift difference is less than the criterion, the galaxy with the photometric redshift is chosen (group C). Then, the magnitude gap (m_{12}) is defined by $m_{12} = r_{2nd} - r_{\rm BCG}$, where $r_{\rm BCG}$ and r_{2nd} are r-band cmodel magnitudes from SDSS for BCG and the 2nd brightest galaxy, respectively.

Figure 2 presents the comparison between the magnitude gap and the cluster central entropy. Filled and open symbols indicate secure (group A) and potential (group B and C) 2nd brightest galaxies, respectively. The color scheme is the same to Figure 1. It seems that m_{12} becomes larger when the central entropy gets smaller or clusters are more relaxed, which is consistent with published results (Smith et al. 2010; Green et al. 2016). Since BCGs in low K_0 clusters are well aligned with the X-ray center and low K_0 corresponds to a strong cool core, if the central entropy represents the maturity of galaxy clusters, the trends in Figure 2 can be attributed to the systematic accretion of the most massive cluster members in the cluster core onto the BCG. In addition, this suggests that m_{12} correlates with the central entropy of the intracluster medium of their host galaxy cluster.

In Figure 2, we can also find exceptional clusters which do not follow the trend (A267 and A2261), i.e., the large magnitude gap (m_{12} >2) and high entropy. The magnitude gap also implies that these clusters are fossil clusters regarded as the most evolved system (Jones et al. 2003). Assuming that both low entropy and the large m_{12} are yardsticks for matured clusters, it is difficult to explain their properties linked to their formation scenarios. For example, the halo merger can alters the entropy from low to high. In fact, A267 has been classified as merging clusters based on their X-ray morphology, although A2261 may be relaxed (Zhang et al. 2008). In Mantz et al. (2015), none of them are classified as relaxed clusters, and 1–2 morphological parameters satisfy their criteria. However, each of these two BCGs has a property consistent with a recent massive merger. In A2261, Postman et al. (2012) find an exceptionally large core radius for the BCG with an offset core "consistent with a local dynamical perturbation of the core". Also, the BCG in A267 shows distinct shells in its outer

[3] http://www.sdss.org/dr12/algorithms/photo-z/

halo in Hubble Space Telescope imaging[4] suggesting a recent galaxy merger. The connection between m_{12} and the growth of the BCG needs a significantly larger sample to establish a definitive link to mergers, the central entropy and the dominance of the brightest galaxy.

3.2. *Red-sequence Members*

Red galaxies in galaxy clusters are mostly composed of old stellar populations. Hence, their colors and magnitudes generate a relation known as the red-sequence (RS). However, an age spread of RS galaxies or infalling of new members in the cluster environment can lead to the color scatter on the sequence. In this section, we investigate the dependence of RS color scatters on the central entropy of galaxy clusters and the composition of stellar population in RS galaxies. For this analysis, BCGs are excluded.

3.2.1. *Color Scatter*

To measure the RS color scatter, we define the red-sequence first. As shown in Figure 3, we use K-corrected colors and absolute magnitude at $z = 0.1$ of member galaxies in all 29 galaxy clusters. This gives an advantage to avoid the effect of redshift dependence of observed galaxy colors. Mean colors of galaxies in each magnitude bin with a 0.5 mag interval are calculated by the 2σ clipping algorithm (red points in Figure 3). Then, we perform the linear fit to the calculated colors and central magnitudes of each bin (red line). The best fit RS is ${}^{0.1}(g-r) = -0.02\,{}^{0.1}M_r + 0.55$. Finally, the Gaussian distribution is fitted to the distribution of color differences between galaxies and the fitted sequence. The final fitting is performed for each galaxy cluster, and we define the RS color scatter ($\sigma_{\rm RS}$) with the standard deviation of the Gaussian fit. We also note that galaxies within $1.5r_{200}$ from the X-ray center and with ${}^{0.1}M_r$ <-20 are used.

Figure 4 shows the scatter against the cluster central entropy. The errors are measured by repeating the bootstrap method 100 times. From Figure 4, there is a cluster-to-cluster variation, but we cannot find significant dependence of $\sigma_{\rm RS}$ on K_0. The Spearman's rank correlation coefficient is 0.22. Furthermore, even if we change the center from the X-ray center to the BCG position, there is still no dependence of the color scatter on the central entropy. This implies that the population of RS galaxies is not to be affected by the central entropy of the intracluster medium.

3.2.2. *Stellar Population*

Previously, we saw that the scatter of RS galaxy colors does not depend on the central entropy of host clusters. Now, we study the stellar population of RS galaxies in different central entropy bins.

We use SDSS spectra to obtain the representative spectra of RS galaxies. To select RS galaxies, we apply a criterion of 0.1 mag bluer than the best fit. In addition, we use RS galaxies with ${}^{0.1}M_r < -21.9$ in order to select RS galaxies with similar masses under the survey depth of SDSS. Using selected RS galaxies, we split them into three groups based on the central entropy of host clusters with K_0 >120, 50< K_0 <120 and K_0 <50 keV cm^2. There are 48, 34 and 29 galaxies from the highest to lowest entropy bins. Although K_0 for the last bin is higher than 30 keV cm^2 mentioned in the previous section, this bin includes Zw2701, whose BCG also shows emission lines. Therefore, all galaxy clusters in the lowest K_0 bin host active BCGs. Then, spectra of RS galaxies in each bin are stacked after deredshifting to the rest-frame and normalizing with the median flux at 5450Å $< \lambda <$ 5550Å. The Galactic extinction is also corrected based on $E(B-V)$ from Schlegel et al. (1998) and the extinction curve from Cardelli et al. (1989) with the update for the near-UV by O'Donnell (1994).

Color coded spectra in left panels of Figure 5 show stacked spectra for each bin. To investigate the stellar population, we run STARLIGHT (Cid Fernandes et al. 2005). We use the library from Bruzual & Charlot (2003) with 6 metallicities (0.005, 0.02, 0.2, 0.4, 1.0, and 2.5 $Z_\odot$) and 13 ages (100 Myr – 13 Gyr). The fitting is repeated 100 times with 100 different random seeds. Black lines in left panels of Figure 5 are best fit examples for each stacked spectrum of RS galaxies. The right panels present stellar mass fractions derived by the mean values of 100 fits as a function of age. The mass fraction for the oldest bin (age>10 Gyr) is over 96 % for all groups. On the other hand, that for younger stellar population (age<2.5 Gyr) is 1.3, 0.7 and 2.5 % for K_0 >120, 50< K_0 <120 and K_0 <50 keV cm^2, respectively. It is clear that there is little difference of stellar populations in bright (${}^{0.1}M_r < -21.9$) RS galaxies with respect to the core properties of their host galaxy cluster, as expected given the relative volume of the cluster core and the cluster as a whole.

However, we note that deep near-UV and mid-IR data can help to divide RS members into two distinct subgroups based on the presence of recent star formation. For instance, Ko et al. (2013, 2016) point out that recent star formation traced by near-UV and mid-IR excess is not negligible among nearby, quiescent early-type galaxies on the tight RS.

3.3. *BCG–Cluster*

The connection between central galaxies and host halos has been regarded as an important subject, since

[4] https://archive.stsci.edu/hst/

galaxies form and evolve in their host halos. In this section, we investigate the dependence of BCG properties, especially related to their mass, on the properties of galaxy clusters. Hereafter, we split BCGs into those in K_0 <50 keV cm^2 clusters (LK-BCGs) and K_0 >50 keV cm^2 clusters (HK-BCGs). Noted that all LK-BCGs show emission lines, but none of HK-BCGs show emission lines.

3.3.1. *Stellar Mass to Cluster Mass*

Figure 6 shows the stellar mass of BCGs ($M_*^{\rm BCG}$) we derived against the central entropy of their host clusters (top). The errorbar indicates the 1σ range of the stellar mass probability distribution. Blue and red points are for LK-BCGs and HK-BCGs, respectively. The stellar masses of LK-BCGs are at the low end regime of the stellar mass distribution of our BCGs. The inset in the top panel presents the stellar mass distribution of BCGs normalized with the peak amplitude of each subsample. Through the Kolmogorov-Smirnov (KS) test, the probability that they are from the same distribution is 0.009.

In Figure 7, we plot $M_*^{\rm BCG}$ as a function of cluster mass, M_{200} (top panels). For comparing our measurement (left) with other works, we also plot the stellar masses derived by different schemes from Maraston et al. (2013) (middle) and MPA/JHU (right). BCGs with spectroscopic information in this work are presented in the left panel, and the cross-matched ones with other literatures are shown in middle and right panels. The color scheme is same to Figure 6. Although it seems less significant in the right panel, our result and Maraston et al. (2013) commonly show that LK-BCGs (blue) have relatively lower stellar masses than HK-BCGs (red). The offset between median $M_*^{\rm BCG}$ values for each subsample are 0.22, 0.42 and 0.09 dex for ours, Maraston et al. (2013) and MPA/JHU, respectively. The horizontal dotted lines are median stellar masses.

Green et al. (2016) demonstrate that BCGs with strong emission lines can have bluer optical or UV/optical colors and redder mid-IR colors than normal passive BCGs. Therefore, this bluer SED by star formation or AGN can lead to lower stellar mass. In fact, most LK-BCGs in this work also have bluer $u-r$ colors. The bottom panel of Figure 6 shows $^{0.1}(u-r)$ color corrected to $z = 0.1$ of BCGs as a function of cluster central entropy. It is apparent that LK-BCGs are bluer than HK-BCGs. In addition, of the eight LK-BCGs included in Kewley et al. (2006), two are classified as LINERs and the rest of them are composite populations from the BPT classification suggesting a mix of star formation and AGN activity.

We also plot the stellar mass to cluster mass ratio ($M_*^{\rm BCG}/M_{200}$), instead of $M_*^{\rm BCG}$, in the bottom panels of Figure 7. The solid lines are the power-law fit results with the bisector algorithm (Isobe et al. 1990) for all (black), LK-BCGs (blue) and HK-BCGs (red). The offset is still evident in the ratio between LK-BCGs and HK-BCGs, and the fitted lines also confirm the discrepancy. However, the relation can also depends on the method used to estimate the stellar mass. The power-law indices for all BCGs are -0.95±0.24, -1.53±0.40 and -0.77±0.36 from left to right panels. Moreover, from previous studies, it was found that the relation between BCG stellar mass and cluster mass is $M_*^{\rm BCG} \propto M_{\rm cl}{}^{(0.12\pm0.03)}$ (Whiley et al. 2008), $M_*^{\rm BCG} \propto M_{500}{}^{(0.78\pm0.06)}$ (Stott et al. 2012) and $M_*^{\rm BCG} \propto M_{500}{}^{(0.34\pm0.11)}$ (Kravtsov et al. 2014), which are converted to the power-law index of -0.88, -0.22 and -0.66 for mass ratio and cluster mass.

3.3.2. σ^{BCG} *vs.* $\sigma^{cluster}$ *Relation*

In the previous section, we demonstrated that the stellar mass of BCGs can depend on their current activity and the relation between stellar mass and cluster mass can vary depending on the methodology used to derive them. In this section, we use another directly observable quantity for an additional comparison, and then discuss what these results imply.

Figure 8 is similar to Figure 6, but now we use the stellar velocity dispersion of BCGs ($\sigma_v^{\rm BCG}$) that is the quantity measured directly from the SDSS spectra. Compared to Figure 6, no dependence to the cluster central entropy or the BCG activity is apparent. This is also seen from the inset that shows the similar distribution of $\sigma_v^{\rm BCG}$ whatever the cluster entropy is. The probability from the KS test is 0.73 which is much higher than that for stellar masses in the previous section.

Again, the top panels of Figure 9 show $\sigma_v^{\rm BCG}$ against M_{200} (left) and the velocity dispersion of host clusters, $\sigma_v^{\rm cl}$ (right). It seems that $\sigma_v^{\rm BCG}$ of LK-BCGs (blue) is similar to that of HK-BCGs (red), which is different from the result based on stellar masses mentioned in the previous section. The difference of median $\sigma_v^{\rm BCG}$ for subsamples (dotted lines) is 0.03 dex. The bottom panels present $\sigma_v^{\rm BCG}/M_{200}$–$M_{200}$ (left) and $\sigma_v^{\rm BCG}/\sigma_v^{\rm cl}$–$\sigma_v^{\rm cl}$ (right). The power-law indices for all BCGs (black solid line) are -1.06±0.08 and -1.16±0.24 for $\sigma_v^{\rm BCG}/M_{200}$ and $\sigma_v^{\rm BCG}/\sigma_v^{\rm cl}$, respectively. In addition, the fitted results for LK-BCGs and HK-BCGs are not significantly different. Interestingly, the indices for all BCGs are indistinguishable from -1, which may indicate the stellar velocity dispersion of BCGs is nearly constant with a scatter whatever cluster masses or velocity dispersions are. However, it is necessary to study the relation with more BCGs over a wider range of cluster mass for a better constraint.

Differently from the stellar mass, the stellar velocity

dispersion is less affected by the dominant light sources such as minor bright young stellar populations or AGN. In addition, McDonald (2011) and McDonald et al. (2016) pointed out that the fuel of star formation in BCGs was galaxy-galaxy interactions at early times, but the main source became inctracluster medium cooling recently. Therefore, the similar $\sigma_v^{\rm BCG}$–$\sigma_v^{\rm cl}$ relation irrespective of the BCG activity implies that the bulk of main stellar body or potential formed at the early epoch and settled down. However, the current activity imprinting emission lines and color excess may be triggered by the intracluster medium recently. Additionally, Hamer et al. (2016) find the rotationally supported gas kinematics at the cluster core which is also decoupled from the stellar component of BCGs. In addition, Rawle et al. (2012) reported the external origin of the cold gas for BCGs and the star formation fueled by the intracluster medium.

The velocity dispersion is a directly observable quantity that reflects the gravitational potential of systems. From this work, the velocity dispersion seems to be less affected by star formation or AGN activity. Wake et al. (2012a,b) pointed out that the velocity dispersion of galaxies is more tightly related to the properties of host dark matter halos and galaxies. Recently, Zahid et al. (2016) also report on the fundamental nature of the central stellar velocity dispersion. Furthermore, since the stellar velocity dispersion is related to the mass of a supermassive black hole residing in the galaxy center (Ferrarese & Merritt 2000; Gebhardt et al. 2000), the relation between $\sigma_v^{\rm BCG}$ and host cluster also provides an opportunity to link supermassive black holes to the cluster scale dark matter halos as well as the relation between central galaxies and their host halos.

Finally, we also note that $\sigma_v^{\rm cl}$ and M_{200} for HeCS clusters were mainly derived using red galaxies. However, as Gal et al. (2008) and Kim et al. (2016) mentioned, there is little evidence that $\sigma_v^{\rm cl}$ from red galaxies only or all cluster members are significantly different due to the state of galaxy clusters at high redshift. Therefore, more clusters at various epochs must be studied to understand the evolution of potential wells of BCGs and clusters, and the interrelation between central galaxies and their host dark matter halos.

4. CONCLUSION

Using 29 galaxy clusters at $0.1< z <0.3$ with extensive spectroscopic coverage from HeCS and X-ray information from ACCEPT, we investigated the dependence of member galaxy properties on host clusters. The main results are as follows:

1. Based on BCGs selected and X-ray information, we confirm the connection between the central entropy (K_0) of clusters and X-ray/BCG offset, meaning that BCGs are well aligned in relaxed clusters. Also, the spatial offset between active BCGs and X-ray centers is $\lesssim$10 kpc.

2. The magnitude difference between BCG and the second brightest one (m_{12}) is also related to K_0. BCGs in matured clusters are more evolved and become dominant. This also indicates that m_{12} correlates with the central properties of the intracluster medium of the cluster.

3. The color scatter of red-sequence member galaxies does not depend on the central entropy of clusters, but shows a substantial cluster-to-cluster variation. This implies that the central entropy of the intracluster medium does not influence the red-sequence members, irrespective of the dynamical state of the cluster on larger scales.

4. BCGs in low entropy clusters (LK-BCGs) showing emission lines are relatively less massive than those in high entropy clusters in terms of the stellar component. This leads to a different $M_*^{\rm BCG}/M_{200}$–M_{200} relation between BCGs related to their level of activity. The low mass of LK-BCGs may be caused by blue spectral energy distribution influenced by minor young massive stars or AGN. Another issue is that different methodologies deriving the stellar mass result in different relations dependent on the presence of recent star formation.

5. In contrast to $M_*^{\rm BCG}$, the stellar velocity dispersion of BCGs ($\sigma_v^{\rm BCG}$) shows no offset between BCGs in high and low entropy clusters. This implies that the main stellar body or potential of BCGs have formed earlier, and the activity of LK-BCGs may be recently triggered by other effects such as the intracluster medium.

Here, we used 29 galaxy clusters at relatively low redshift. However, the evolution of galaxy clusters and galaxies is more active in the early universe. Hence, it is necessary to use more BCGs at various epochs to understand the evolutionary features. This will provide interesting information about the evolution of gravitational potential for galaxies and dark matter halos, and the relation between them. Moreover, since low mass galaxies play a more important role to build up the red-sequence (e.g., De Lucia et al. 2004), it is also worth to understand the population of low mass cluster galaxies.

Authors thank anonymous referee for comments improving this manuscript. A.C.E. acknowledges support

from STFC grant ST/L00075X/1. SDSS-III is managed by the Astrophysical Research Consortium for the Participating Institutions of the SDSS-III Collaboration including the University of Arizona, the Brazilian Participation Group, Brookhaven National Laboratory, Carnegie Mellon University, University of Florida, the French Participation Group, the German Participation Group, Harvard University, the Instituto de Astrofisica de Canarias, the Michigan State/ Notre Dame/JINA Participation Group, Johns Hopkins University, Lawrence Berkeley National Laboratory, Max Planck Institute for Astrophysics, Max Planck Institute for Extraterrestrial Physics, New Mexico State University, New York University, Ohio State University, Pennsylvania State University, University of Portsmouth, Princeton University, the Spanish Participation Group, University of Tokyo, University of Utah, Vanderbilt University, University of Virginia, University of Washington, and Yale University. This research has made use of the NASA/IPAC Extragalactic Database (NED) which is operated by the Jet Propulsion Laboratory, California Institute of Technology, under contract with the National Aeronautics and Space Administration.

Facilities: SDSS, MMT(Hectospec)

Software: FAST, STARLIGHT

REFERENCES

Adelman-McCarthy, J. K., Agüeros, M. A., Allam, S. S., et al. 2008, ApJS, 175, 297
Alam, S., Albareti, F. D., Allende Prieto, C., et al. 2015, ApJS, 219, 12
Baugh, C. M. 2006, RPPh, 69, 3101
Beck, R., Dobos, L., Budavári, T., Szalay, A. S., & Csabai, I. 2016, MNRAS, 460, 1371
Behroozi, P. S., Conroy, C., & Wechsler, R. H. 2010, ApJ, 717, 379
Blanton, M. R., Eisenstein, D., Hogg, D. W., Schlegel, D. J., & Brinkmann, J. 2005a, ApJ, 629, 143
Blanton, M. R., & Roweis, S. 2007, AJ, 133, 734
Blanton, M. R., Schlegel, D. J., Strauss, M. A., et al. 2005b, AJ, 129, 2562
Bruzual, G., & Charlot, S. 2003, MNRAS, 344, 1000
Calzetti, D., Armus, L., Bolhlin, R. C., et al. 2000, ApJ, 533, 682
Cardelli, J. A., Clayton, G. C., & Mathis, J. S. 1989, ApJ, 345, 245
Cavagnolo, K. W., Donahue, M., Voit, G. M., & Sun, M. 2008, ApJL, 683, L107
Cavagnolo, K. W., Donahue, M., Voit, G. M., & Sun, M. 2009, ApJ, 182, 12
Chabrier, G. 2003, PASP, 115, 763
Cid Fernandes, R., Mateus, A., Sodré, L., Stasińska, G., & Gomes, J. M. 2005, MNRAS, 358, 363
Conroy, C., Gunn, J. E., & White, M. 2009, ApJ, 699, 486
Crawford, C. S., Allen, S. W., Ebeling, H., Edge, A. C., & Fabian, A. C. 1999, MNRAS, 306, 857
De Lucia, G., Poggianti, B. M., Aragón-Salamanca, A., et al. 2004, ApJL, 610, L77
Donahue, M., Bruch, S., Wang, E., et al. 2010, ApJ, 715, 881
Diaferio, A. 1999, MNRAS, 309, 610
Diaferio, A., & Geller, M. J. 1997, ApJ, 481, 633
Edge, A. C. 2001, MNRAS, 328, 762
Edge, A. C., Ivison, R. J., Smail, I., Blain, A. W., & Kneib, J. -P. 1999, MNRAS, 306, 599
Edge, A. C., Oonk, J. B. R., Mittal, R., et al. 2010, A&A, 518, L46
Edge, A. C., Wilman, R. J., Johnstone, R. M., et al. 2002, MNRAS, 337, 49
Egami, E., Rieke, G. H., Fadda, D., & Hines, D. C. 2006, ApJL, 652, L21
Ferrarese, L., & Merritt, D. 2000, ApJL, 539, L9
Fogarty, K., Postman, M., Connor, T., Donahue, M., & Moustakas, J. 2015, ApJ, 813, 117
Gal, R. R., Lemaux, B. C., Lubin, L. M., Kocevski, D., & Squires, G. K. 2008, ApJ, 684, 933
Gebhardt, K., Bender, R., Bower, G., et al. 2000, ApJL, 539, L13
Gonzalez, A. H., Zaritsky, D., & Zabludoff, A. I. 2007, ApJ, 666, 147
Green, T. S., Edge, A. C., Stott, J. P., et al. 2016, MNRAS, 461, 560
Groenewald, D. N., & Loubser, S. I. 2014, MNRAS, 444, 808
Hamer, S. L., Edge, A. C., Swinbank, A. M., et al. 2016, MNRAS, 460, 1758
Hansen, S. M., Sheldon, E. S., Wechsler, R. H., & Koester, B. P. 2009, ApJ, 699, 1333
Hashimoto, Y., Henry, J. P., & Boehringer, H. 2014, MNRAS, 440, 588
Hoffer, A. S., Donahue, M., Hicks, A., & Barthelemy, R. S. 2012, ApJS, 199, 23
Hwang, H. S., Geller, M. J., Park, C., et al. 2016, ApJ, 818, 173
Hwang, H. S., Elbaz, D., Lee, J. C., Jeong, W.-S., Park, C., Lee, M. G., & Lee, H. M. 2010, A&A, 522, 33
Hwang, H. S., Park, C., Elbaz, D., & Choi, Y. -Y. 2012, A&A, 538, 15
Isobe, T., Feigelson, E. D., Akritas, M. G., & Babu, G. J. 1990, ApJ, 364, 104
Jones, L. R., Ponman, T. J., Horton, A., Babul, A., Ebeling, H., & Burke, D. J. 2003, MNRAS, 343, 627
Katayama, H., Hayashida, K., Takahara, F., & Fujita, Y. 2003, ApJ, 585, 687
Kauffmann, G., Heckman, T. M., White, S. D. M., et al. 2003, MNRAS, 341, 33
Kewley, L. J., Groves, B., Kauffmann, G., & Heckman, T. 2006, MNRAS, 372, 961
Kravtsov, A., Vikhlinin, A., & Meshscheryakov, A. 2014, arXiv:1401.7329
Kim, J. -W., Im, M., Lee, S. -K., et al. 2015, ApJ, 806, 189
Kim, J. -W., Im, M., Lee, S. -K., et al. 2016, ApJL, 821, L10
Kriek, M., van Dokkum, P. G., Labbé, I., et al. 2009, ApJ, 700, 221
Ko, J., Hwang, H. S., Lee, J. C., & Sohn, Y. -J. 2013, ApJ, 767, 90
Ko, J., Chung, H., Hwang, H. S., & Lee, J. C. 2016, ApJ, 820, 2
Kroupa, P. 2001, MNRAS, 322, 231
Lauer, T. R., Postman, M., Strauss, M. A., Graves, G. J., & Chisari, N. E. 2014, ApJ, 797, 82
Lin, Y. -T., & Mohr, J. J. 2004, ApJ, 617, 879
Loh, Y. -S., & Strauss, M. A. 2006, MNRAS, 366, 373

Mantz, A. B., Allen, S. W., Morris, R. G., Schmidt, R. W., von der Linden, A., & Urban, O. 2015, MNRAS, 449, 199
Maraston, C., Pforr, J., Henriques, B. M., et al. 2013, MNRAS, 435, 2764
McDonald, M., Stalder, B., Bayliss, M., et al. 2016, ApJ, 817, 86
McDonald, M. 2011, ApJL, 742, L35
Mittal, R., Oonk, J. B. R., Ferland, G. J., et al. 2012, MNRAS, 426, 2957
Montero-Dorta, A. D., Shu, Y., Bolton, A. S., Brownstein, J. R., & Weiner, B. J. 2016, MNRAS, 456, 3265
Moster, B. P., Somerville, R. S., Maulbetsch, C., et al. 2010, ApJ, 710, 903
Pipino, A., Szabo, T., Pierpaoli, E., MacKenzie, S. M., & Dong, F. 2011, MNRAS, 417, 2817
Postman, M., Lauer, T. R., Donahue, M., et al. 2012, ApJ, 756, 159
O'Donnell, J. E. 1994, ApJ, 422, 158
Ostriker, J. P., & Tremaine, S. D. 1975, ApJL, 202, L113
Rafferty, D. A., McNamara, B. R., & Nulsen, P. E. J. 2008, ApJ, 687, 899
Rawle, T. D., Edge, A. C., Egami, E., et al., 2012, ApJ, 747, 29
Rines, K., Geller, M. J., Diaferio, A., & Kurtz, M. J. 2013, ApJ, 767, 15
Salomé, P., & Combes, F. 2003, A&A, 412, 657
Salpeter, E. E. 1955, ApJ, 121, 161
Sanderson, A. J. R., Edge, A. C., & Smith, G. P. 2009, MNRAS, 398, 1698
Schlegel, D. J., Finkbeiner, D. P., & David, M. 1998, ApJ, 500, 525
Serra, A. L., Diaferio, A., Murante, G., & Borgani, S. 2011, MNRAS, 412, 800
Smith, G. P., Khosroshahi, H. G., Dariush, A., et al. 2010, MNRAS, 409, 169
Stott, J. P., Hickox, R. C., Edge, A. C., et al. 2012, MNRAS, 422, 2213
Tegmark, M., Blanton, M. R., Strauss, M. A., et al. 2004, ApJ, 606, 702
Voges, W., Aschenbach, B., Boller, Th., et al. 1999, A&A, 349, 389
Wake, D. A., Franx, M., & van Dokkum, P. G. 2012a, arXiv:1201.1913
Wake, D. A., van Dokkum, P. G., & Franx, M. 2012b, ApJL, 751, L44
Wake, D. A., Whitaker, K. E., Labbé, I., et al. 2011, ApJ, 728, 46
Wang, J., Overzier, R., Kauffmann, G., von der Linde, A., & Kong, X. 2010, MNRAS, 401, 433
Whiley, I. M., Aragón-Salamanca, A., De Lucia, G., et al. 2008, MNRAS, 387, 1253
White, S. D. M., & Rees, M. J. 1978, MNRAS, 183, 341
Zahid, H. J., Geller, M. J., Fabricant, D. G., & Hwang, H. S. 2016, ApJ, 832, 203
Zhang, Y. Y., Finoguenov, A., Böhringer, H., Kneib, J. -P., Smith, G. P., Kneissl, R., Okabe, N., & Dahle, H. 2008, A&A, 482, 451
Zheng, Z., Coil, A. L., & Zehavi, I. 2007, ApJ, 667, 760

Table 1. Summary of galaxy clusters used in this work.

Cluster	X-ray Coordinates[a]		z[b]	r_{200}[b]	M_{200}[b]	$\sigma_v^{\rm cl}$[b]	K_0[a]	Morph.[c]
	R.A. (J2000)	decl. (J2000)		(Mpc)	($10^{14} M_\odot$)	(km s^{-1})	(keV cm^2)	
A267	01:52:42.27	+01:00:45.33	0.2291	1.19	4.95±0.31	972^{+63}_{-53}	168.56	A
A697	08:42:57.55	+36:21:57.65	0.2812	1.13	4.42±2.10	1002^{+97}_{-75}	166.67	SA
MS0906	09:09:12.75	+10:58:32.00	0.1767	0.81	1.47±0.19	664^{+87}_{-62}	104.23	n/a
A773	09:17:52.57	+51:43:38.18	0.2173	1.40	7.84±0.10	1110^{+86}_{-70}	244.32	SA
Zw2701	09:52:49.18	+51:53:05.27	0.2160	0.86	1.83±0.54	652^{+74}_{-55}	39.66	SPA
A963	10:17:03.74	+39:02:49.17	0.2041	1.12	4.01±0.05	956^{+80}_{-64}	55.77	SA
Zw3146	10:23:39.74	+04:11:08.05	0.2894	1.00	3.11±1.41	858^{+103}_{-75}	11.42	PA
A1068	10:40:44.52	+39:57:10.28	0.1386	1.47	8.40±0.66	1028^{+106}_{-81}	9.11	SPA
A1201	11:12:54.49	+13:26:08.76	0.1671	0.99	2.66±0.06	683^{+68}_{-53}	64.81	A
A1204	11:13:20.42	+17:35:38.45	0.1706	0.74	1.11±0.14	532^{+62}_{-46}	15.31	SPA
A1361	11:43:39.64	+46:21:20.41	0.1159	0.78	1.25±0.00	512^{+64}_{-47}	18.64	n/a
A1413	11:55:17.89	+23:24:21.84	0.1412	1.29	5.72±0.02	856^{+90}_{-68}	64.03	SA
A1423	11:57:17.26	+33:36:37.44	0.2142	1.09	3.68±0.06	759^{+64}_{-51}	68.32	S
A1689	13:11:29.61	-01:20:28.69	0.1842	1.46	8.68±2.64	1197^{+78}_{-65}	78.44	SA
A1758	13:32:48.40	+50:32:32.53	0.2760	0.90	2.23±0.75	674^{+99}_{-69}	230.84	n/a
A1763	13:35:17.96	+40:59:55.80	0.2312	1.62	12.40±1.39	1261^{+81}_{-68}	214.69	0
A1835	14:01:01.95	+02:52:43.18	0.2506	1.41	8.41±0.53	1151^{+80}_{-66}	11.44	SPA
A1914	14:26:03.06	+37:49:27.84	0.1660	1.20	4.77±0.13	798^{+53}_{-44}	107.16	A
RXJ1504	15:04:07.42	-02:48:15.70	0.2168	0.91	2.16±1.51	779^{+105}_{-75}	13.08	SPA
A2034	15:10:12.50	+33:30:39.57	0.1132	1.25	5.03±0.05	942^{+64}_{-53}	232.64	SA
A2069	15:24:11.38	+29:52:19.02	0.1139	1.39	6.96±0.08	994^{+61}_{-52}	453.25	n/a
A2111	15:39:40.64	+34:25:28.01	0.2291	1.00	2.90±0.35	741^{+65}_{-52}	107.36	0
A2187	16:24:14.02	+41:14:37.53	0.1829	0.77	1.27±0.16	631^{+83}_{-59}	78.63	n/a
A2219	16:40:20.11	+46:42:42.84	0.2257	1.46	8.98±2.42	1151^{+63}_{-54}	411.57	SA
A2259	17:20:08.30	+27:40:11.53	0.1605	1.12	3.84±0.68	855^{+76}_{-60}	113.98	SA
RXJ1720	17:20:09.94	+26:37:29.11	0.1604	1.18	4.47±0.30	860^{+40}_{-35}	21.03	SPA
A2261	17:22:27.25	+32:07:58.60	0.2242	0.97	2.62±0.91	780^{+78}_{-60}	61.08	SA
RXJ2129	21:29:39.94	+00:05:18.83	0.2339	1.24	5.59±1.16	858^{+71}_{-57}	21.14	SPA
A2631	23:37:38.56	+00:16:05.02	0.2765	1.07	3.80±0.84	851^{+96}_{-72}	308.81	0

[a] Values based on the ACCEPT data (Cavagnolo et al. 2009)

[b] Values based on the HeCS data (Rines et al. 2013)

[c] X-ray morphological parameters satisfying the criteria in Mantz et al. (2015). The parameters of S, P and A indicate symmetry, peakiness and alignment, respectively. 0 means that all parameters do not satisfy the criteria. If there is no measurement from Mantz et al. (2015), we note n/a.

Table 2. Summary of BCGs and the 2nd brightest galaxies defined in this work. Column (2-3) give the coordinate of BCGs, and column (4) lists the offset between positions of BCG and the X-ray center. Column (5) is the stellar mass derived in this work. Column (6) is the stellar velocity dispersion of BCGs described in § 2.3. Column (7-8) give the coordinate of the 2nd brightest galaxies, and column (9) is the magnitude difference between BCGs and the 2nd brightest galaxies. The final column indicates how the 2nd brightest one was selected (see the text). It is noted that we do not present values if they are unavailable.

Cluster	BCG Coordinates		Offset	$\log M_*^{\rm BCG}$	$\sigma_v^{\rm BCG}$	2nd Brightest		m_{12}	Group
	R.A. (J2000)	decl. (J2000)	(kpc)	($M_\odot$)	(km s^{-1})	R.A. (J2000)	decl. (J2000)	(mag)	
A267	01:52:42	+01:00:26	74.46	$12.42^{+0.01}_{-0.02}$	297±16	01:52:22	+01:00:08	2.2558	A
A697	08:42:58	+36:21:59	6.85	$11.81^{+0.11}_{-0.42}$	-	08:42:58	+36:22:01	0.4992	B
MS0906	09:09:13	+10:58:29	8.71	$12.02^{+0.11}_{-0.19}$	341±18	09:09:07	+10:57:51	0.6064	A
A773	09:17:53	+51:43:37	43.91	$12.19^{+0.00}_{-0.02}$	-	09:17:53	+51:44:01	0.6228	B
Zw2701	09:52:49	+51:53:05	1.28	$11.95^{+0.23}_{-0.08}$	298±15	09:53:01	+51:52:25	1.4925	A
A963	10:17:04	+39:02:49	5.58	$12.18^{+0.02}_{-0.02}$	330±14	10:17:22	+39:00:07	1.1557	A
Zw3146	10:23:40	+04:11:11	13.12	$11.11^{+0.21}_{-0.03}$	229±22	10:23:37	+04:09:06	1.3916	A
A1068	10:40:44	+39:57:11	2.55	$11.85^{+0.07}_{-0.21}$	-	10:40:34	+40:03:49	1.5706	A
A1201	11:12:55	+13:26:09	0.88	$12.03^{+0.32}_{-0.41}$	267±14	11:12:50	+13:28:30	1.4455	A
A1204	11:13:21	+17:35:41	8.29	$11.67^{+0.14}_{-0.60}$	260±14	11:13:32	+17:38:42	0.9101	A
A1361	11:43:40	+46:21:20	1.15	$11.80^{+0.16}_{-0.49}$	262±20	11:44:00	+46:24:23	1.0571	C
A1413	11:55:18	+23:24:18	10.83	$12.12^{+0.09}_{-0.24}$	-	11:54:58	+23:25:20	1.6880	A
A1423	11:57:17	+33:36:39	7.29	$11.94^{+0.11}_{-0.18}$	-	11:57:36	+33:34:39	1.3500	C
A1689	13:11:30	-01:20:28	5.18	$12.05^{+0.03}_{-0.05}$	-	13:11:30	-01:20:43	0.2307	C
A1758	13:32:52	+50:31:34	334.75	$11.83^{+0.13}_{-0.18}$	245±23	13:32:41	+50:33:46	0.6007	A
A1763	13:35:20	+41:00:04	120.44	$12.07^{+0.10}_{-0.23}$	-	13:34:54	+40:56:55	0.2665	A
A1835	14:01:02	+02:52:42	7.46	$11.72^{+0.24}_{-0.55}$	221±18	14:01:07	+02:50:55	1.6744	A
A1914	14:25:57	+37:48:59	280.82	$11.91^{+0.13}_{-0.18}$	274±13	14:26:04	+37:49:53	0.8563	A
RXJ1504	15:04:08	-02:48:17	5.89	$11.34^{+0.20}_{-0.62}$	326±30	15:04:23	-02:47:29	1.7690	A
A2034	15:10:12	+33:29:11	183.11	$11.89^{+0.17}_{-0.47}$	-	15:10:20	+33:29:10	0.8965	A
A2069	15:24:07	+29:53:20	175.46	$11.93^{+0.04}_{-0.61}$	241±12	15:24:08	+29:52:55	0.6387	A
A2111	15:39:40	+34:25:27	8.25	$11.72^{+0.17}_{-0.36}$	261±22	15:39:42	+34:24:43	0.1720	A
A2187	16:24:14	+41:14:38	1.24	$12.03^{+0.08}_{-0.19}$	292±18	16:24:23	+41:15:37	1.0774	A
A2219	16:40:20	+46:42:41	16.86	$11.74^{+0.09}_{-0.20}$	-	16:40:32	+46:42:30	0.7224	C
A2259	17:20:10	+27:40:08	56.25	$12.13^{+0.02}_{-0.03}$	-	17:20:11	+27:42:14	1.0062	A
RXJ1720	17:20:10	+26:37:32	9.12	$11.82^{+0.05}_{-0.31}$	273±15	17:20:32	+26:40:20	0.9514	A
A2261	17:22:27	+32:07:57	6.11	$12.39^{+0.02}_{-0.03}$	386±19	17:22:35	+32:07:44	2.1591	A
RXJ2129	21:29:40	+00:05:21	8.68	$11.82^{+0.18}_{-0.13}$	285±20	21:29:36	+00:01:29	1.0558	C
A2631	23:37:40	+00:16:17	89.11	$11.97^{+0.06}_{-0.45}$	289±18	23:37:24	+00:16:21	0.5863	A

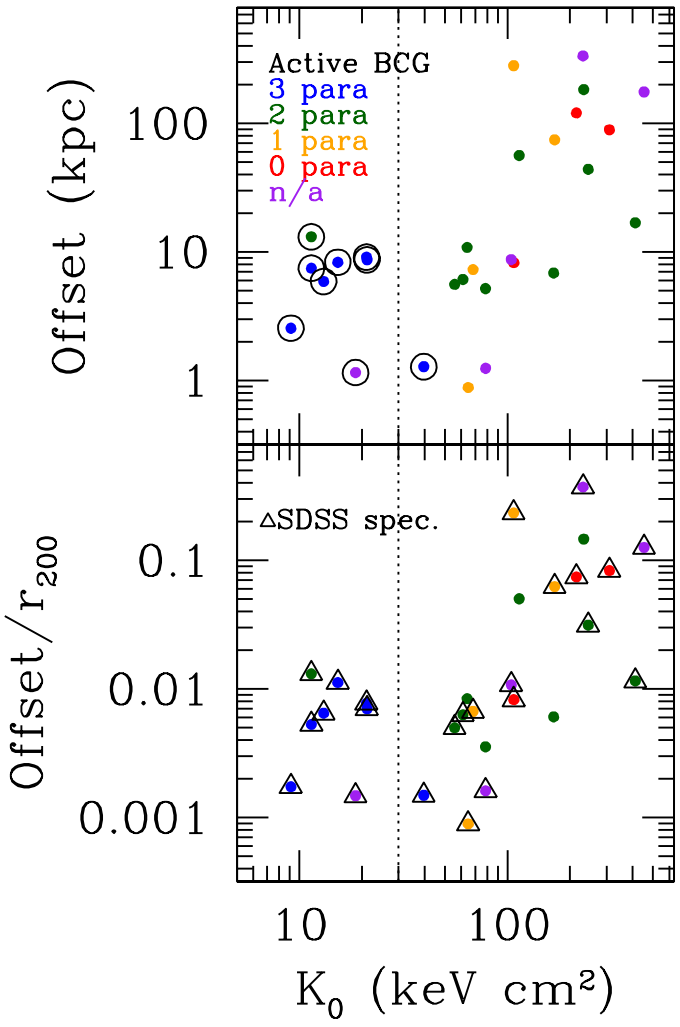

Figure 1. The projected X-ray/BCG offset (top) and the offset normalized by cluster radius (bottom) versus central entropy for 29 galaxy clusters in this work. Open circles in the top panel indicate BCGs with emission lines. The color code presents the number of X-ray morphological parameters satisfying the criteria in Mantz et al. (2015). Open triangles in the bottom panel are for BCGs with SDSS spectra. The dotted line shows the value of K_0 =30 keV cm^2 that distinguish galaxy clusters hosting active and passive BCGs (Cavagnolo et al. 2008). The BCGs in high K_0 galaxy clusters tend to be more misaligned.

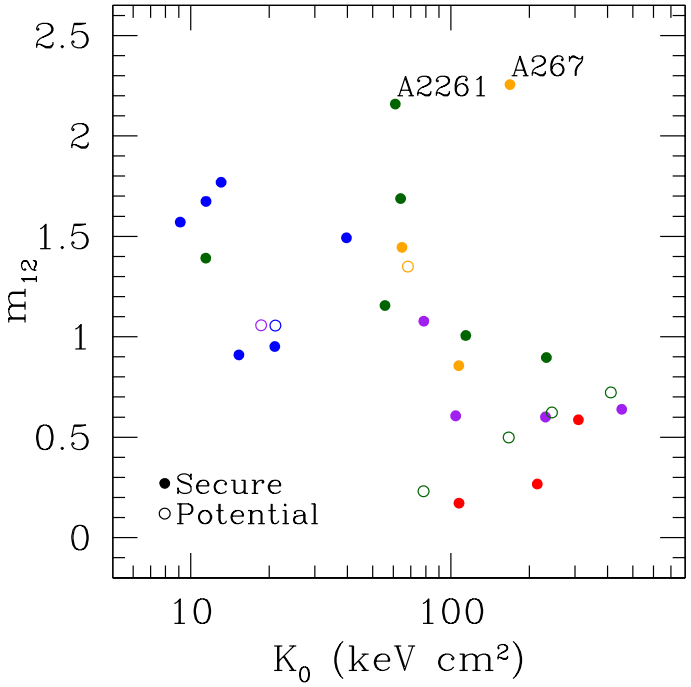

Figure 2. The magnitude difference between BCG and the 2nd brightest galaxy against the central entropy of clusters. The color code is the same to Figure 1. Filled and open circles indicate securely confirmed 2nd brightest galaxies and potential ones, respectively (see the text for more details). The anti-correlation between two parameters appears, i.e., m_{12} gets larger as the entropy decreases. We also label two exceptional clusters which do not follow the trend.

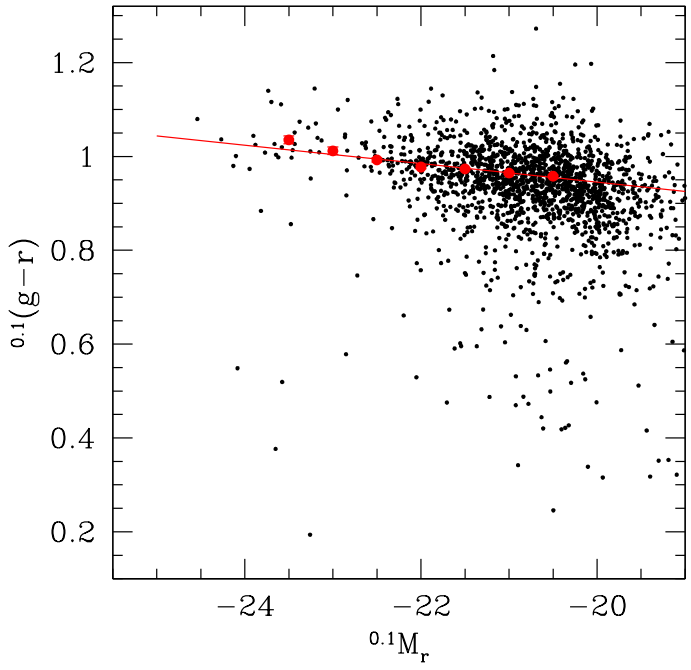

Figure 3. The color-magnitude diagram of spectroscopically confirmed member galaxies in 29 galaxy clusters. Red points show mean colors in each magnitude bin, and the red line is the defined red-sequence.

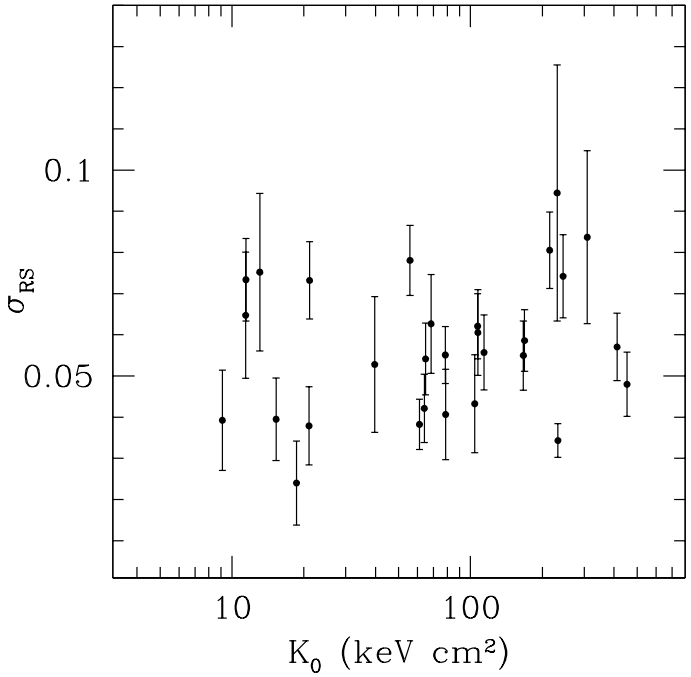

Figure 4. The $^{0.1}(g-r)$ scatter of red-sequence galaxies with $M_r < -20$ and within $1.5r_{200}$ from the X-ray center. There is no clear dependence of scatters on the central entropy of galaxy clusters.

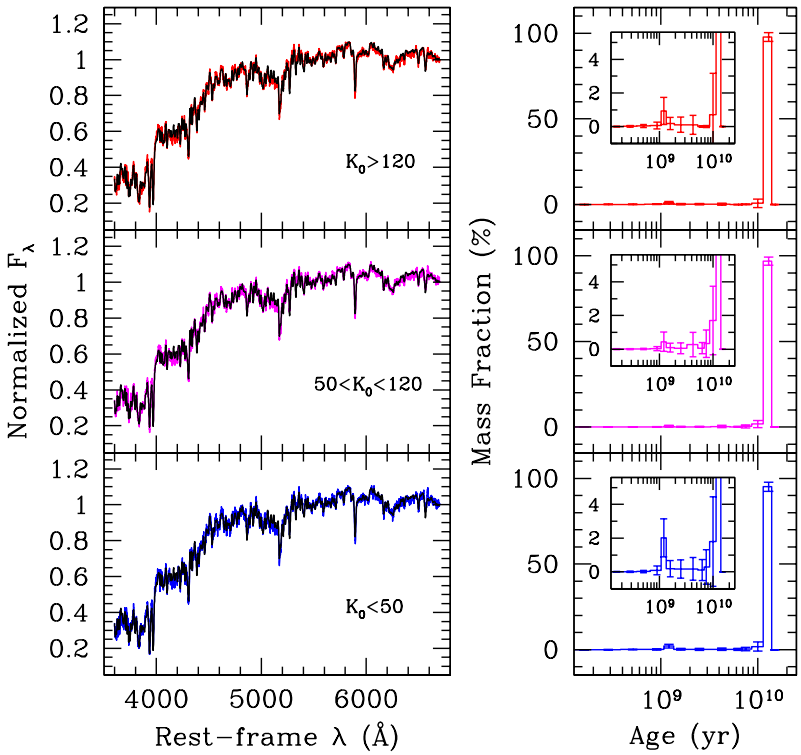

Figure 5. The stacked SDSS spectra (left) of red-sequence galaxies with $M_r < -21.9$ and within $1.5r_{200}$ from the X-ray center. The galaxy clusters are split into three K_0 bins, and black lines show examples of best fit results from the STARLIGHT code. The right panel shows the stellar mass fraction of stellar populations with different ages. The insets are zoomed one showing the fraction of younger populations. There is no significant difference on the stacked spectrum and stellar population composition.

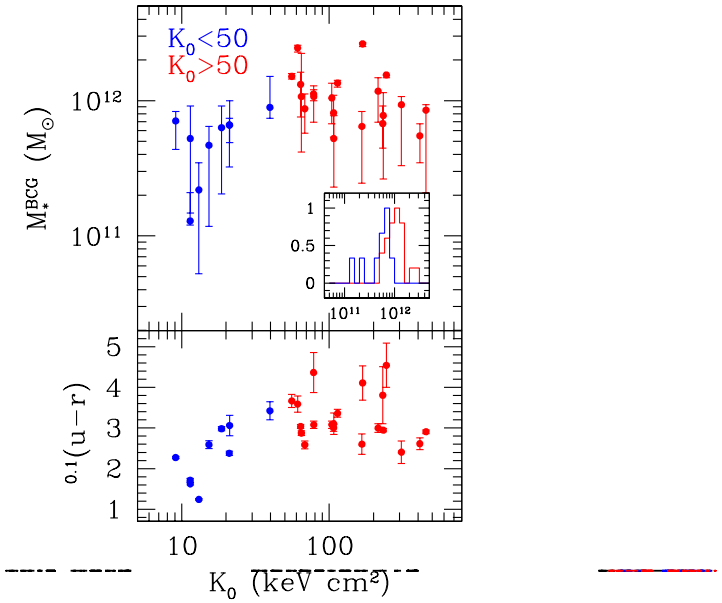

Figure 6. Stellar mass of BCGs against the central entropy of galaxy clusters studied in this work (top). Blue and red points are BCGs for K_0 <50 and K_0 >50 keV cm^2, respectively. The inset in the top panel shows the stellar mass distribution of each subsample normalized with the peak amplitude. The stellar masses of BCGs in low K_0 clusters are distributed at the low end regime. The bottom panel is for $^{0.1}(u-r)$ color of BCGs, which shows BCGs in low K_0 clusters also tend to be bluer.

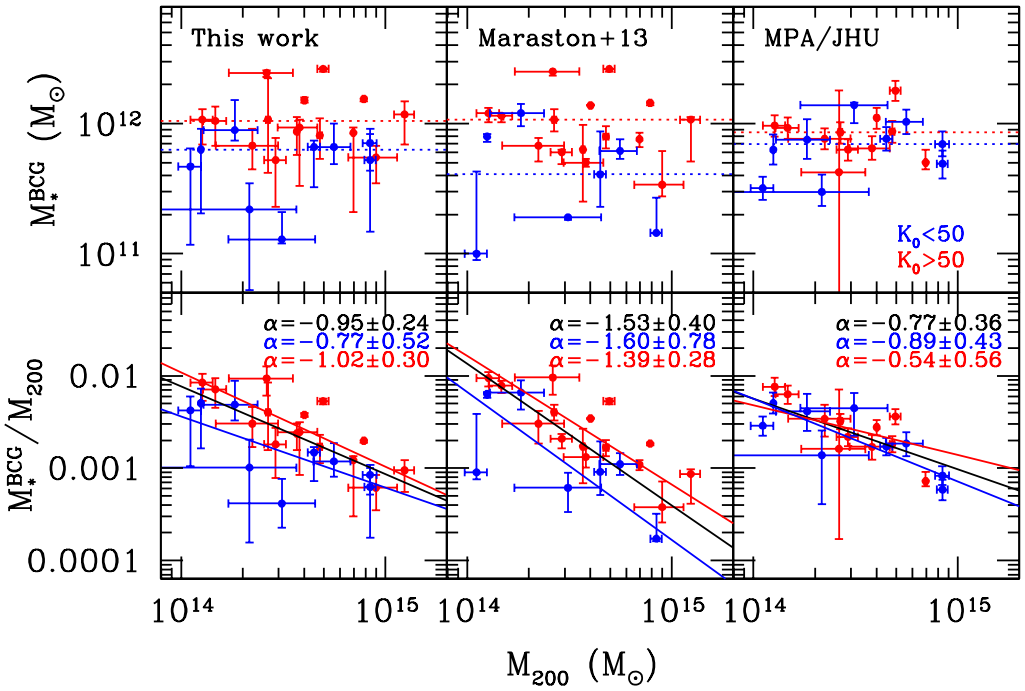

Figure 7. Stellar mass (top) and stellar mass-to-cluster mass ratio (bottom) of BCGs against cluster masses. The results of stellar masses derived by this work (left), Maraston et al. (2013) (middle) and MPA/JHU (right) are compared. The color scheme is same to Figure 6. Dotted lines in the top panels indicate the median values of each subsample with the same color scheme. The stellar mass of BCGs in low entropy clusters can be relatively lower than BCGs in high entropy clusters, although this may be affected by how the stellar mass is measured. The solid lines in bottom panels are best fit power-law for all (black), LK-BCGs (blue) and HK-BCGs (red). The noted values in each bottom panel are power-law indices of $M_*^{\rm BCG}/M_{200} \propto M_{200}{}^{\alpha}$ for each subsample.

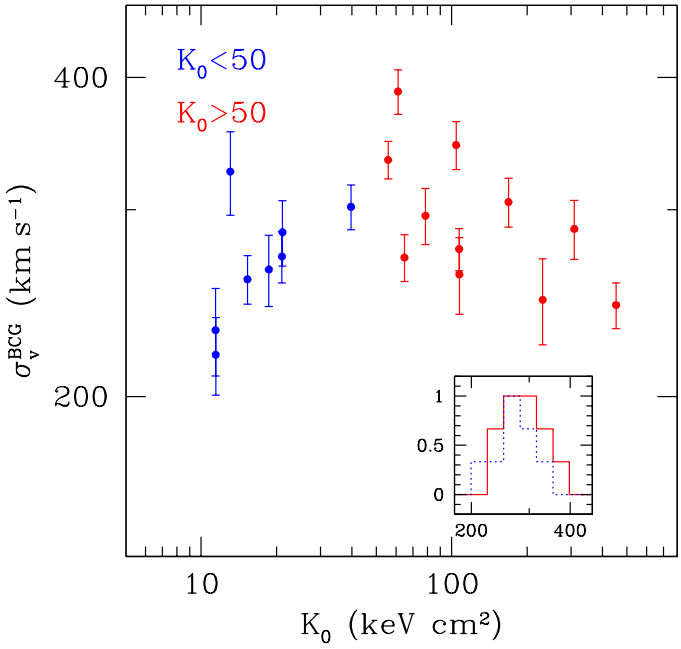

Figure 8. Similar figure to Figure 6 with the same color, but the stellar velocity dispersion of BCGs is used. Compared to Figure 6, the offset of $\sigma_v^{\rm BCG}$ for BCGs in low K_0 clusters is not significant.

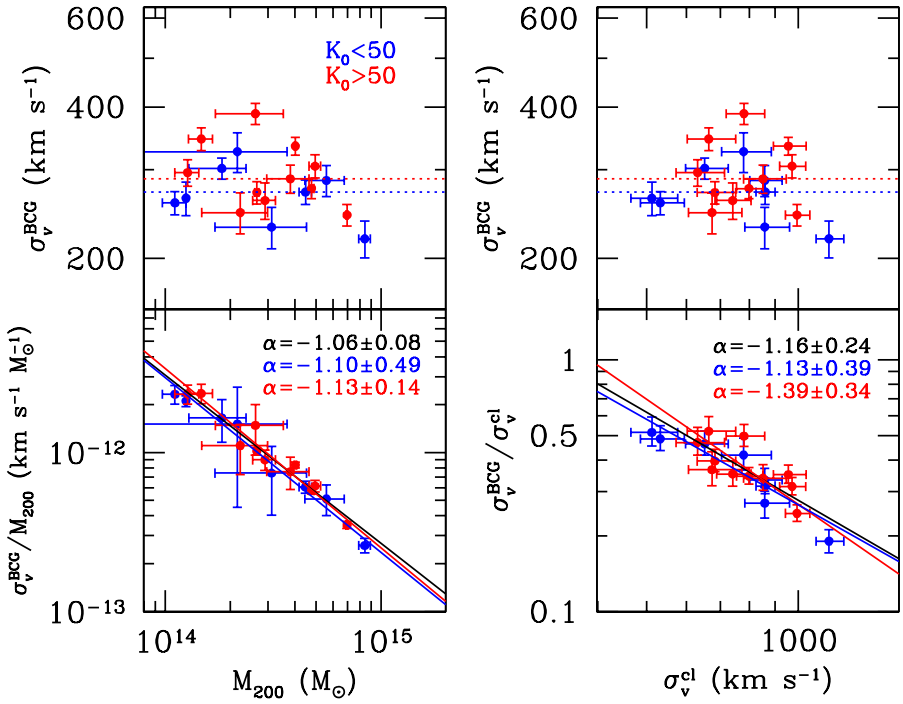

Figure 9. Similar figure to Figure 7 with the same color scheme, but the velocity dispersions of BCGs is used instead of stellar masses (left). In the right panel, the velocity dispersion of galaxy clusters is used rather than the cluster mass. Independently of BCG activity, there is no significant offset between subsamples, especially in terms of the ratio. The noted values in each bottom panel are power-law indices of $\sigma_{\rm v}^{\rm BCG}/M_{200} \propto M_{200}{}^{\alpha}$ (left) and $\sigma_{\rm v}^{\rm BCG}/\sigma_{\rm v}^{\rm cl} \propto \sigma_{\rm v}^{\rm cl}{}^{\alpha}$ (right) for each subsample. Noted that BCGs with spectra from SDSS are displayed.